

# Nanoscale

Accepted Manuscript



This is an *Accepted Manuscript*, which has been through the Royal Society of Chemistry peer review process and has been accepted for publication.

*Accepted Manuscripts* are published online shortly after acceptance, before technical editing, formatting and proof reading. Using this free service, authors can make their results available to the community, in citable form, before we publish the edited article. We will replace this *Accepted Manuscript* with the edited and formatted *Advance Article* as soon as it is available.

You can find more information about *Accepted Manuscripts* in the [Information for Authors](#).

Please note that technical editing may introduce minor changes to the text and/or graphics, which may alter content. The journal's standard [Terms & Conditions](#) and the [Ethical guidelines](#) still apply. In no event shall the Royal Society of Chemistry be held responsible for any errors or omissions in this *Accepted Manuscript* or any consequences arising from the use of any information it contains.



## Ultrathin Efficient Perovskite Solar Cell Employing Periodic Structure of Composite Hole Conductor for Elevated Plasmonic Light Harvesting and Hole Collection

Received 00th January 20xx,  
Accepted 00th January 20xx

DOI: 10.1039/x0xx00000x

www.rsc.org/

Mingzhu Long,<sup>a, ‡</sup> Zefeng Chen,<sup>a, ‡</sup> Tiankai Zhang,<sup>a</sup> Yubin Xiao,<sup>a</sup> Xiaoliang Zeng,<sup>b</sup> Jian Chen,<sup>c</sup> Keyou Yan,<sup>a, \*</sup> Jianbin Xu<sup>a, \*</sup>

We develop a molecule/polymer composite hole transporting material (HTM) with periodic microstructure for morphology replication of corrugated Au electrode, which in combination plays dual role in the optical and electronic enhancement for high performance perovskite solar cell (PSC). The electro-optics revealed that perovskite couldn't readily extinct the red light even though the thickness increased to 370 nm, but we found that the quasi periodic microstructure composite (PMC) HTM in combination with the conformal Au electrode could promote the absorption through the enhanced cavity effects, leading to comparable absorption even using much thinner perovskite (240 nm). We identified the cavity was the combination of Fabry–Pérot interferometer and surface plasmonic resonance, with light harvesting enhancement through surface plasmon polariton or waveguide modes that propagate in the plane of the perovskite layer. On the other hand, the PMC HTM increased hole conductivity by one order of magnitude with respect to standard spiro-OMeTAD HTM due to molecular packing and self-assembly, embodying traceable hole mobility and density elevation up to 3 times, and thus the hysteresis was greatly avoided. Thanks to dually optical and electronic enhancement, the PMC PSC afforded high efficiency PSC using as thin as 240 nm perovskite layer, delivering a  $V_{oc}$  of 1.05 V,  $J_{sc}$  of 22.9 mA cm<sup>-2</sup>, FF of 0.736, and efficiency amounting to 17.7% PCE, the highest efficiency with ultrathin perovskite layer.

### Introduction

The interest in the development of the organo-metal halide perovskite solar cells (PSCs) is mainly driven by its unique electronic properties, including the high carrier mobility and long range balanced diffusion length.<sup>1-11</sup> In terms of light harvesting, perovskite can readily capture the photons when  $\lambda < 500$  nm, while external quantum efficiency (EQE) between 500 nm and 800 nm is strongly dependent on the perovskite quality and thickness owing to quick drop of extinction coefficient when  $\lambda \geq 500$  nm.<sup>12-15</sup> For, example, 180 nm thick perovskite film can extinct all the blue light but 500 nm thick film can't fully capture the red light (e.g. 760 nm), thereby EQE curve of PSC generally falls rapidly after 500 nm.<sup>16</sup> Therefore, device optimization for maximizing photon harvesting in the red region is extremely important for high efficiency PSCs, which can provide the possibility to approach the theoretical

photocurrent.<sup>17-19</sup> Since the increasing of physical thickness will certainly reduce the charge collection efficiency and/or result in large abnormal *J-V* hysteresis, it's also practicable to enhance the light absorption (optical thickness) through light management instead of thickness increase. As well known, plasmonic noble metal nanostructure and light cavities are two typical concepts to repopulate light field and enhance the light trapping, which are thereby expected to improve the red light extinction in solar cells. The former, antenna-like metal nanostructure, can amplify 4-5 orders of magnitude local electromagnetic field through localized surface plasmonic resonance (LSPR) at some specific wavelengths, typically at 430 nm and 530 nm for gold.<sup>20-23</sup> However, this narrow band response doesn't permit enough extra light harvesting in solar spectrum. Therefore, it's rarely realized by applying noble metal particle for light management in PSC to date.<sup>24, 25</sup> The latter, especially with periodic microstructure textured/embedded as 3D cavity, is another widely-used candidate to enhance the light trapping effect in thin film based solar cells and new generation solar cell,<sup>26-29</sup> which can provide broadband enhancement through surface plasmon polariton (SPP) or waveguide (SPW) modes. However, it's still difficult to embed or texture additional periodic microstructure inside a 300~500 nm thick PSC film, without any hindering the deposition process for high quality photoactive layer. Based on this preliminary consideration, we intend to build a periodic microstructure of hole transporting

<sup>a</sup> Department of Electronic Engineering, The Chinese University of Hong Kong, Hong Kong, SAR, P. R. China.

<sup>b</sup> Shenzhen Institute of Advanced Technology, Chinese Academy of Science, Shenzhen, 518055, P. R. China.

<sup>c</sup> Instrumental Analysis and Research Center, Sun Yat-sen University, Guangzhou, 510275, P. R. China.

† E-mail: yankeyou@gmail.com; jbxu@ee.cuhk.edu.hk

Electronic Supplementary Information (ESI) available: XRD patterns corresponding to the perovskite; AFM images of 3D PMC HTM perovskite solar cell; Performance statistics for 3D PMC HTM; Ultraviolet photoelectron spectra (UPS) of HTMs on FTO. See DOI: 10.1039/x0xx00000x

material (HTM) during the deposition process and then replicate a periodic metallic back electrode atop, which can serve as efficient grating-coupler SPR cavity and thus increase light trapping in PSC.

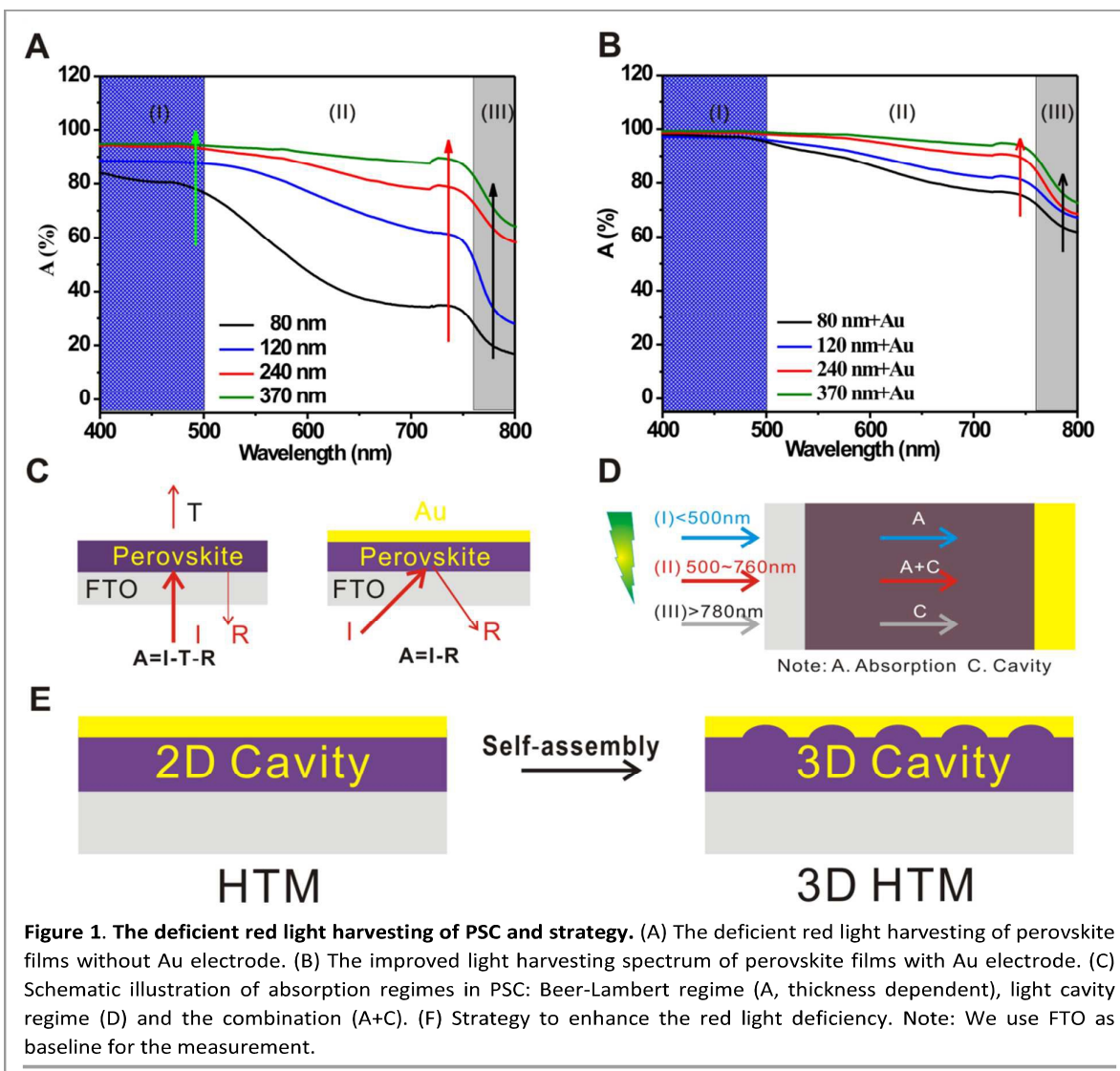
With regard to HTM, spiro-OMeTAD is widely employed in solid state dye sensitized solar cell and perovskite solar cell due to good interface with light absorbing layer and high hole mobility. This good interface is achieved during the deposition process and simultaneously the convex-concave absorbing layer was leveled up to a flatten film.<sup>30</sup> In contrast, the polymeric hole conductors (well-known PTAA) tend to keep the surface morphology of perovskite film, showing pillared structures as reflective mirror for increasing light harvesting.<sup>31</sup> The main distinction arises from that more easily infiltrating property of the small molecular HTM spiro-OMeTAD than the high-molecular-weight polymer. Therefore, it's possible to combine molecule HTM with polymer HTM to engineer the interface with perovskite and conform convex-concave surface morphology below, achieving high hole extraction and efficient light harvesting simultaneously. Moreover, the interaction between molecule and polymer was able to self-assemble into various morphologies in selective solvents and/or arrange into crystalline structure on the substrate, which provide possibility to devise surface morphology and optimize to 3D periodic microstructure. This morphology assembly is quite useful and reports have revealed that self-assembly induced molecular arrangement/packing could lead to the mobility increase by orders of magnitude, and thus it merits attention and benefits a lot for PSC if high hole collection could be achieved.<sup>32, 33</sup>

In this work, we successfully fabricated a molecule/polymer periodic microstructure composite (PMC) HTM embossment and deposited morphological replication of Au electrode atop. The PMC HTM was achieved by self-assembling of the typical molecular HTM (spiro-OMeTAD) and polymeric HTM (P3HT) on the perovskite layer during the deposition process. The size and pitch of embossment were facily controlled through the component volumetric ratio of binary HTM precursor solutions and optimized to 3:1 combination ratio of spiro-OMeTAD/P3HT. We demonstrated that PMC HTM delivered both optical and electronic enhancement accounting for the high performance. First, the PMC HTM in combination with conformally corrugated Au electrode afforded enhanced light cavity effects, promoting the absorption, and thus even much thinner perovskite (240 nm) led to high absorption. The light cavity worked in the combination of Fabry-Pérot interferometer and SPR, coupling light into surface plasmon polariton or photonic modes and propagating along in-plane of perovskite layer for long optical thickness. Second, the hole conductivity of PMC increased one order of magnitude with respect to standard spiro-OMeTAD HTM due to molecular packing and self-assembly, with traceable hole mobility and density elevation up to 3 times, and thus the hysteresis was greatly reduced. Therefore, the short current  $J_{sc}$  and overall performance was greatly increased through the optimized PMC HTM. We got the PMC PSC with PCE up to 16.3% and

17.7% in forward scan and reverse scan, respectively, with short current as high as  $\sim 22.9 \text{ mA cm}^{-2}$  approaching to its theoretical value and  $\sim 88\%$  spectrally flat EQE using  $\sim 240 \text{ nm}$  thick perovskite films. Due to ease of fabrication and performance improvement, the PMC paves the venue towards high efficient PSCs using ultrathin active layer through photonic management and electronic amelioration.

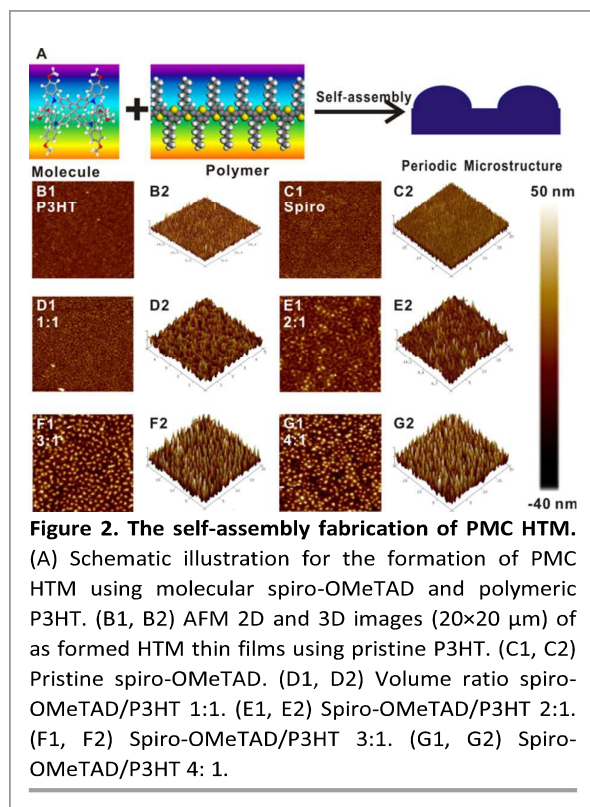
## RESULTS AND DISCUSSION

**Deficient Red Light Absorption of perovskite films.** Figure 1A and 1B display the absorptance of perovskite thin films with different thicknesses before and after gold coating. Before gold coating, we can see that perovskite can absorb short wavelength light easily (green arrow) but can't extinct long wavelength light completely (red arrow and black arrow) at all. For example, as thin as 120 nm perovskite film can absorb 90% blue light but allow 50% transmittance at 760 nm (see Figure 1A). Even increasing thickness to 370 nm, there is 30% unabsorbed red light at 760 nm. After coating of 100 nm gold electrode, the absorption is greatly increased. 80 nm perovskite film has similar absorptance to 370 nm when  $< 500 \text{ nm}$  and its absorptance at 760 nm increase from 20% to 70% after Au coating. Hence, the 240 nm perovskite film has nearly complete absorption in all the visible range in the aid of gold film, which reduces physical thickness but it increases optical thickness. The increased absorption can be attributed to light cavity effect, which has been demonstrated in the planar electrodes recently.<sup>16</sup> As well known, this sandwiched active layer has thickness comparable to sub-wavelength, which is indeed possible to promote the absorption due to the light interference in combination with plasmonic electrode. Figure 1C presents the absorption measurement without/with Au electrode using equation ( $A=I-T-R$ , Left;  $A=I-R$ , Right, I: incidence, A: absorption, T: transmittance, R: reflectance). Therefore, we roughly summarize the absorption regimes from Figure 1A and 1B after the comparison: Beer-Lambert absorption regime (A,  $< 500 \text{ nm}$ ), the perovskite absorption is highly thickness-dependent; cavity regime (C,  $> 780$ ), the light is trapped inside and repopulated; and the combination (A+C,  $500 \sim 780 \text{ nm}$ ), the light absorption highly relies on cavity promotion (Figure 1D). Simplistically speaking, the PSC is strongly absorbing in the former regime and weakly absorbing in the latter, but the latter can promote the absorption of the former in not necessary and sufficient condition. Hence, based on the absorption curve, one can predict that the EQE should be fully saturated even for thin perovskite junctions ( $< 180 \text{ nm}$ ) for  $\lambda < 500 \text{ nm}$  but it's really difficult to saturate in more thick perovskite film ( $> 500 \text{ nm}$ ) if without cavity promotion (e.g. carbon back electrode system).<sup>34-37</sup> Therefore, it's crucial to enhance the cavity effects through surface corrugation, namely using PMC for 3D light cavity (Figure 1F), which is chemically implemented in this work.



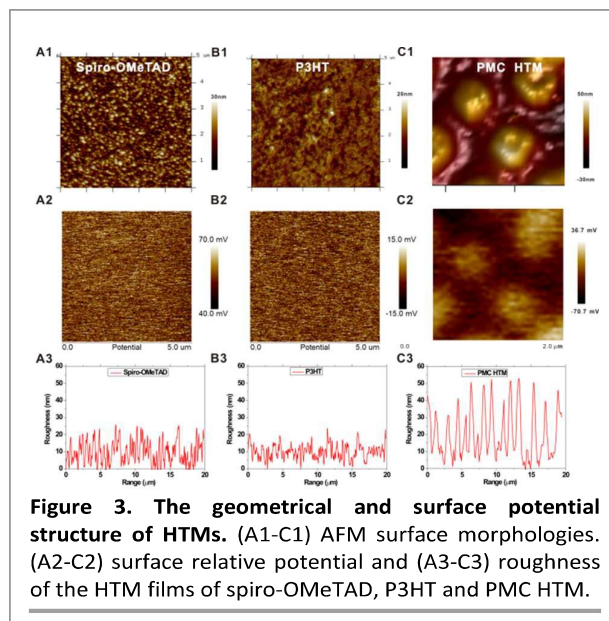
**Fabrication of PMC HTM for 3D Optical Cavity.** It's still difficult to embed or texture additional periodic microstructure inside a 300~500 nm thick PSC, without any hindering the deposition process of ultrathin and unstable photoactive layer. We build a periodic microstructure HTM during the deposition process first and then replicate a periodic metallic back electrode atop, which can serve as efficient SPR cavity and thus increase light trapping in PSC. We implement the fabrication through molecular packing and self-assembly in a molecule/polymer composite system. Figure 2 presents the overall fabrication of PMC HTM through ratio control in binary system. We separately prepared 15 mg mL<sup>-1</sup> P3HT in 1, 2 dichlorobenzene (DCB) and 75 mg mL<sup>-1</sup> spiro-OMeTAD with the basic additives in chlorobenzene (CB) that are usually employed in the PSCs as stock solution.<sup>7, 38</sup> The binary HTM precursors were then prepared through blending different volume ratios of the two solutions and used to deposit corresponding HTM layers. The basic formation is schematically illustrated in Figure 2(A), which is a self-assembly process for embossment formation to combine molecular spiro-OMeTAD with polymeric P3HT,

accompanied with ratio dependent morphology tuning for an optimum microstructure. Figure 2B-2G present these morphologies of thin films prepared by different binary HTM ratios in large area (20 μm), which contain basic formation information of self-assembly process. Both of pristine HTM films display uniform coverage and smooth surface on FTO substrate in the zoom-out thumbnail (see Figure 2B and 2C), and can be regarded as 2D HTM structure. Therefore, there is still lack of assembly thermodynamics in single HTM. However, the binary system accelerates self-assembly process towards 3D structure due to their interaction. At 1:1 spiro-OMeTAD/P3HT, the HTM film begins to present chain-shaped nanostructure, which can't be observable in pristine HTMs on the same scale and is regarded as the aggregation of linear polymer P3HT in the presence of spiro-OMeTAD. When combination ratio spiro-OMeTAD/P3HT increases to 2:1, not only even larger nanochains appear but also another micro-embossments come out, sporadically dispersed on the nanochain-interwove surface (see Figure 2E1 and 2E2), which should be spiro-OMeTAD-rich aggregation judged from dot



morphology. At 3:1 of spiro-OMeTAD/P3HT, large amount of spiro-OMeTAD-rich embossments spring up and assembles to quasi-periodic structure of HTM (Figure 2F1 and 2F2). The average diameter of embossments is around 400-600 nm from the AFM images and their pitch is around 1.0 μm ( $P=1.0 \mu\text{m}$ ) and thereby can be defined as typical 3D PMC HTMs. The further increasing the ratio of spiro-OMeTAD/P3HT (4:1) will densify the embossments, leading to a reduced pitch (Figure 2G1 and 2G2). This information further suggests that the embossment should be indeed spiro-OMeTAD-rich aggregation since the more spiro-OMeTAD, the more embossments appear.

The exact assembly mechanism isn't quite clear at present but can be regarded as cross self-assembly process due to morphology differed from separate pristine HTMs. The solubility difference and their interaction is one of possible reasons for self-assembly process from 2D HTM towards 3D HTM. The solubility of P3HT ( $M_w > 65,600 \text{ g mol}^{-1}$ ) is around 50  $\text{mg mL}^{-1}$  in chlorobenzene and dichlorobenzene. Yet the value for spiro-OMeTAD in the same solvent is around 380  $\text{mg mL}^{-1}$ , around 7.5 times larger than that of P3HT. The large difference of the solubility enables sequential precipitation of P3HT and spiro-OMeTAD and phase separation during solvent evaporation after spin coating. In the combined binary system, the P3HT firstly nucleates and precipitates during the solvent evaporation due to lower solubility and then spiro-OMeTAD, resulting in formation of spiro-OMeTAD-rich embossment on the P3HT surface. Spiro-OMeTAD tends to form embossment aggregation probably due to the strong  $\pi$ - $\pi$  interaction in the presence of P3HT. It is worth to mention that there is no



Tyndall effect observed in the binary system when a laser passing through the solution, which suggests that assembly process didn't occur in the solution but during the spin-coating deposition process. Based on binary HTM system, the embossment size and pitch can be facily controlled by tuning the binary composition of the polymer and small molecule, which actually offers a template for gold back electrode during the fabrication process and bring about plasmonic cavity effect without hindering the ultrathin photoactive layer (300 nm) like using imprinting. In the following, we select 3:1 spiro-OMeTAD/P3HT for the detailed optical investigation due to the most periodic arrangement.

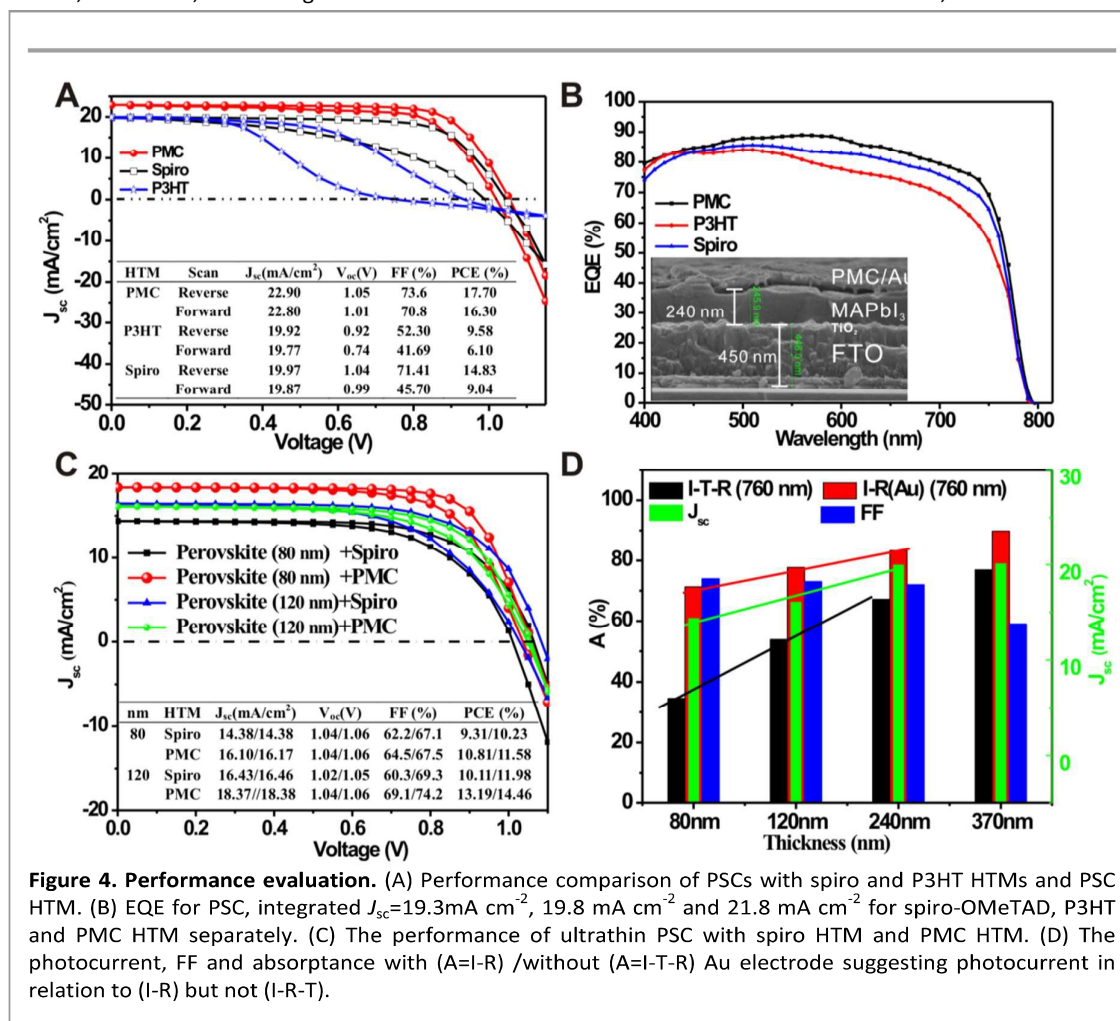
Figure 3 dissects the morphology and structure information of three HTM layers, with the higher resolution AFMs, surface potential mappings as well as surface roughness characterization. First, through high resolution AFMs, the fine structure of the pristine systems also became observable. Spiro-OMeTAD thin film displays small dot-shape morphology (Figure 3A1) and P3HT has nanochain morphology (Figure 3B1), which are consistent with their molecular structures (see Figure 2A left), respectively. Second, the embossment diameter (400-600 nm) and pitch (1.0 μm) can be verified in 3D AFM (Figure 3C1), in association with nanoscale fine roughness of the thin film surface on the convex and concave, thus an ideal hierarchical periodic microstructure for light trapping. Third, the two pristine HTMs (Figure 3A2 to 3B2) have uniform surface potential mapping, whereas surface potential distribution of the PMC structure (Figure 3C2) is closely associated with surface topology, namely, with obvious potential difference between concave and convex. This information suggests that the composition between concave and convex are different, supporting the aforementioned claim that the embossment is mainly consist of spiro-OMeTAD that are evenly dispersed on P3HT-rich film. Moreover, the large potential difference suggests that the binary system actually forms a quasi-potential well for holes in the 3D HTM film for

hole transfer accelerating than that in 2D structure, which will be discussed in the following.<sup>39</sup> Figure 3A3 to 3C3 display the surface roughness in large area for comparison, which clearly demonstrates the PMC properties and provides more visible structure information.

**Enhanced Performance of PMC PSCs.** Based on the fabrication of HTMs, the solar cell performances with different HTM layers are evaluated accordingly. Figure 4A directly compares the performance of 240 nm thick PSCs with three HTMs: Spiro-OMeTAD, P3HT and PMC HTM. As a typical control experiment, the device with spiro-OMeTAD 2D HTM produces  $V_{oc} = 1.04$  V,  $J_{sc} = 19.97$  mA cm<sup>-2</sup>, FF = 0.714 in reverse scan, and  $V_{oc} = 0.99$  V,  $J_{sc} = 19.87$  mA cm<sup>-2</sup>, FF = 0.46 in forward scan, and amounting to 14.83% and 9.04% PCE, respectively, with a mean PCE of 11.94%. P3HT shows much lower performance, that was  $V_{oc} = 0.92$  V,  $J_{sc} = 19.92$  mA cm<sup>-2</sup>, FF = 0.52, and overall PCE = 9.58% in reverse scan, and  $V_{oc} = 0.74$  V,  $J_{sc} = 19.77$  mA cm<sup>-2</sup>, FF = 0.42, overall PCE = 6.10% in forward scan, which can be attributed to less perfect interface and energy alignment between polymer and perovskite. However, the binary PMC HTM has much better performance than the two former HTMs. As shown in **Figure 4A**, it produces  $V_{oc} = 1.01$  V,  $J_{sc} = 22.8$  mA cm<sup>-2</sup>, FF = 0.708, amounting PCE to 16.3% in forward

scan, and  $V_{oc} = 1.05$  V,  $J_{sc}$  as high as 22.9 mA cm<sup>-2</sup>, FF = 0.737, PCE 17.7% in reverse scan, with mean PCE of 17.0% as well as minimum hysteresis. It's worthy to mention that this large photocurrent is produced in ultrathin perovskite layer (240 nm, **Figure 4B** inset), which actually reduces the physical thickness without hindering the optical thickness, indicating high charge collection. In order to understand the enhancement of light harvesting and probe the photon-to-electron conversion, the EQE is measured for comparison. One can see that P3HT based PSCs displays lower EQE in the overall spectral range than spiro-OMeTAD and PMC HTM, which indeed illustrates that P3HT has worse interface than the other two and beyond discussion in the following. The interesting fact is that PMC HTM yields much higher EQE than spiro-OMeTAD, especially in the red range, which suggests that PMC HTM can enhance the photon harvesting through light cavity effect when  $\lambda > 500$  nm as aforementioned and elevate charge collection in the whole spectral range through electronic improvement as well. We finally integrates the  $J_{sc}$  from the EQE spectrum, which are 19.3 mA cm<sup>-2</sup>, 19.8 mA cm<sup>-2</sup> and 21.8 mA cm<sup>-2</sup> for spiro-OMeTAD, P3HT and PMC HTM, respectively, with similar variation tendency to that in the  $J$ - $V$  curves.

In order to confirm the results, we list more thickness-



dependent performance with much thinner perovskites using spiro-OMeTAD HTM and PMC HTM (Figure 4C). Using 80 nm perovskite, spiro-OMeTAD based PSC produces  $V_{oc} = 1.04/1.06$  V,  $J_{sc} = 14.38/14.38$  mA cm<sup>-2</sup>, FF = 0.622/0.671, amounting PCE to 9.31%/10.23% in forward/reverse scan, and PMC PSC increases to  $V_{oc} = 1.04/1.06$  V,  $J_{sc} = 16.10/16.17$  mA cm<sup>-2</sup>, FF = 0.645/0.675, PCE 10.81%/11.8% in forward/reverse scan. Using 120 nm perovskite, spiro-OMeTAD based PSC produces  $V_{oc} = 1.02/1.05$  V,  $J_{sc} = 16.43/16.45$  mA cm<sup>-2</sup>, FF = 0.603/0.693, amounting PCE to 10.11%/11.98% in forward/reverse scan, but PMC PSC yields as high as  $V_{oc} = 1.04/1.06$  V,  $J_{sc} = 18.37/18.38$  mA cm<sup>-2</sup>, FF = 0.691/0.742, PCE 13.19%/14.46% in forward/reverse scan. Generally, PMC PSCs have 2-3 mA cm<sup>-2</sup> larger photocurrents than PSCs using spiro-OMeTAD. In order to correlate performance with light cavity effect, we list the photocurrent of PSCs, absorbance without/with Au electrode in different thicknesses (Figure 4D). We can see that  $J_{sc}$  has more relevance to the absorbance of perovskite with Au electrode than that without gold electrode (see green line and blue line) below 200 nm, which means PMC Au electrode really promotes the absorption, namely, plasmonic cavity enhanced absorption regime in the system. The rougher of Au electrode it is, the larger absorption enhancement will gain in PMC PSC. Therefore, based on the performance analysis, we can preliminarily conclude that both optical enhancement (red light conversion) and electric enhancement (whole light conversion) account for the improved performance and in the following we will sequentially illustrate the mechanics in depth.

**Electro-Optics of 3D PMC PSC.** Before we discuss the light cavity effect of PSC using different HTMs, we first check the physical structure of the devices. Figure 5A displays the device cross-section architectures with different HTM layers. It's easy to see that molecular spiro-OMeTAD can fill and level up the perovskite concave-convex, resulting in a smooth surface due to its small size (Figure 5A top), whereas the large polymer P3HT can't smooth the uneven surface perfectly, leaving a relative rough surface (Figure 5A middle). In the binary HTM system, from the image of exfoliated gold film overlaid on PMC HTM, we can see that bowl-shaped fluctuation formed at the interface with structure corresponding well to the AFM images. Therefore, PMC HTM provides additional roughness to gold electrode induced by embossment, which can offer better light harvesting for photoactive layer (Figure 5A bottom). Figure 5B directly displays the Fabry-Pérot cavity effect from the absorption spectrum without Au electrode in the infrared range, with distinct oscillated absorption due to constructive/destructive interference. The perovskite/spiro-OMeTAD has narrow and regular half peak width due to two flat reflecting surface of perovskite film whereas perovskite/P3HT and perovskite display broad but random half peak width due to the random surface corrugated convex-concave. For the perovskite/PMC film, similar wide and regular half peak width can be observed, thanks to the periodic self-assembly of HTM embossment. This Fabry-Pérot cavity will couple with plasmonic working modes in the following because they both associated with light scattering.

To evaluate the plasmonic cavity effects of Au layers on the different HTMs, we employed relative scattering spectra (RS) using a planar gold film on FTO as reference ( $RS=R\%/R\%_{Ref}$ ) with incident light from gold side (Figure 5C). We can see that the surface plasmon resonance peak at 535 nm can be observed due to the amplification of PMC cavity with regard to spiro-OMeTAD/Au. This optical amplification can be further demonstrated. The effect of mutational step at 720 nm caused by shifting light detector can't be exempted by the normalization using RS of planar gold film due to additional amplification by the 3D plasmonic structure, as the same step in the planar spiro-OMeTAD/Au electrode can be well offset after the normalization. The coupling of light to SPP or SPW modes can be judged from sawtooth in the RS curve of PMC/Au electrode (such as at 574 nm, 675 nm and 840 nm), which allow the propagating of vertical incident light along the lateral and increase the effective travel path. Therefore, the periodic microstructure acts as effective antennas to perform localized SPR (535 nm) for the incident light and also as optical cavity for long range light population (amplification feature and sawtooth feature), amounting to plasmonic cavity effect for efficient light trapping, as schematically illustrated in Figure 5D.<sup>40</sup>

In order to demonstrate the plasmonic cavity effect of periodic microstructure caused by the plasmonic light coupling and hybridization, we employed a rigorous theoretical simulation to study the SPR case in PSC devices with plasmonic structure at the interface of HTM and gold electrode. To simplify the simulation process, the simulated structural parameters are fixed, except using different pitches ( $P=0.3, 0.6, 0.7, 0.8, 0.9$ ,

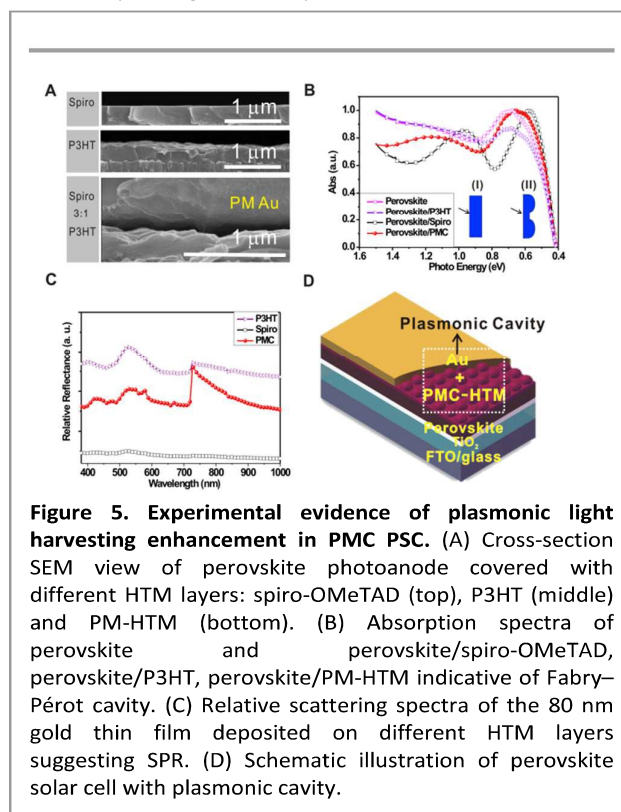


**Figure 5. Experimental evidence of plasmonic light harvesting enhancement in PMC PSC.** (A) Cross-section SEM view of perovskite photoanode covered with different HTM layers: spiro-OMeTAD (top), P3HT (middle) and PM-HTM (bottom). (B) Absorption spectra of perovskite and perovskite/spiro-OMeTAD, perovskite/P3HT, perovskite/PM-HTM indicative of Fabry-Pérot cavity. (C) Relative scattering spectra of the 80 nm gold thin film deposited on different HTM layers suggesting SPR. (D) Schematic illustration of perovskite solar cell with plasmonic cavity.

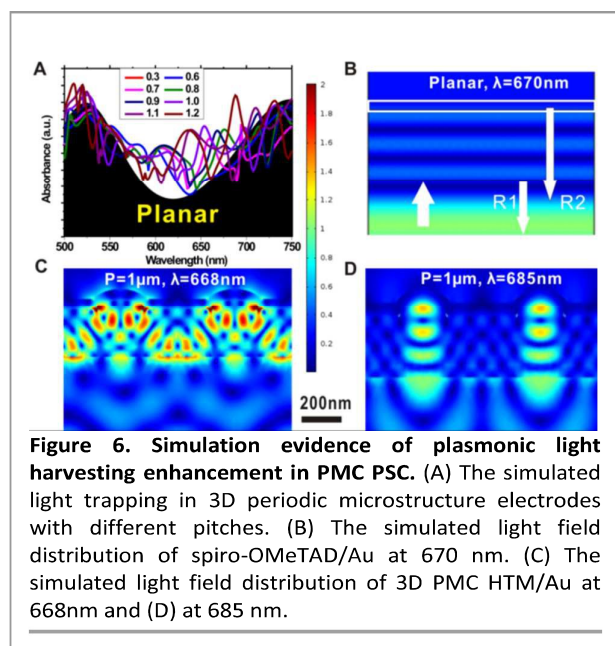


**Figure 6. Simulation evidence of plasmonic light harvesting enhancement in PMC PSC.** (A) The simulated light trapping in 3D periodic microstructure electrodes with different pitches. (B) The simulated light field distribution of Spiro-OMeTAD/Au at 670 nm. (C) The simulated light field distribution of 3D PMC HTM/Au at 668 nm and (D) at 685 nm.

1.0, 1.1 to 1.2  $\mu\text{m}$ ). The micro-bumps height is 80 nm, embossment domain diameter 0.45  $\mu\text{m}$  similar to the actual PMC HTM, and the permittivity (2.1 for the organic and perovskite with the frequency in the terahertz) with an ideal periodic structure. The simulated light trapping curves of the PSC devices are shown in Figure 6A.<sup>29, 41, 42</sup> We can see that PMC 3D electrodes demonstrates several narrow resonance peaks from 550 nm to 750 nm and can compensate the absorption valley of planar electrode devices by enhanced light trapping effect. However, in planar electrode devices, interference fringes suggests that electric field cannot be effectively confined within the absorbing layer and the light reflection (R1 and R2) will lead to coherent light enhancement outside perovskite layer (Figure 6B). However, for periodic microstructure electrodes, at 668 nm, plasmonic resonance employs the SPP/SPW modes to confine the electromagnetic field along the ups and downs of back electrode in the absorbing layer by the periodic geometrics, not only reducing light loss outside the photoactive layer but also populating the light field within the perovskite (Figure 6C). Figure 6D presents the simulated localized plasmonic mode at 685 nm, which shows light localization by the individual convex reflector (Au embossment). Based on the simulation, we conclude that periodic microstructure can be applied to perform effective light engineering in the PSC, thereby ameliorating the light distribution and promoting the light extinction of perovskite.

**The Hole Collection of 3D PMC PSC.** Although the optical enhanced absorption can explain the EQE increasing in the red, the whole enhancement in all the range should be attributed to electronic ameliorating. The improved hole extraction can be determined by space charge limit current (SCLC) in hole only devices. Figure 7A and 7B are the basic results without/with perovskite employing Spiro, P3HT and PMC HTMs. When operating in the space charge limit current (SCLC) regime, the dark current of the hole only device was well

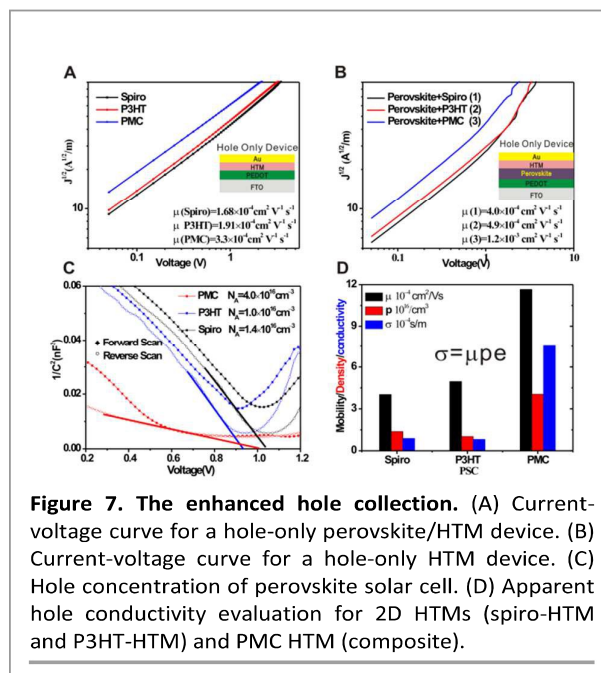


**Figure 7. The enhanced hole collection.** (A) Current-voltage curve for a hole-only perovskite/HTM device. (B) Current-voltage curve for a hole-only HTM device. (C) Hole concentration of perovskite solar cell. (D) Apparent hole conductivity evaluation for 2D HTMs (Spiro-HTM and P3HT-HTM) and PMC HTM (composite).

abided by the Mott-Gurney law:  $J = 9\epsilon\epsilon_0\mu V^2/8L^3$ . Hole motilities of pristine HTMs are  $1.68 \times 10^{-4}$ ,  $1.91 \times 10^{-4}$  and  $3.3 \times 10^{-4} \text{ cm}^2/\text{Vs}$  for Spiro, P3HT and PMC, respectively, with an increasing factor of 2 after assembly from single component HTM to PMC. After incorporating on the perovskite, apparent hole motilities elevate to  $4.0 \times 10^{-4}$ ,  $4.9 \times 10^{-4}$  and  $1.2 \times 10^{-3} \text{ cm}^2/\text{Vs}$  for Spiro, P3HT and PMC, with one order of magnitude, which can be attributed to the interwoven interface with perovskite.

We applied Mott-Schottky analysis of capacitance-voltage measurement to extract hole density and the built-in voltage.<sup>43</sup> Based on the  $1/C^2$ -V curves with reverse scan in Figure 7C, the carrier density can be obtained referring to the slope  $k$  and equation  $1/N_0 = ke \epsilon \epsilon_0 A^2/2$ .<sup>44</sup> It is obviously shown in the curves that the hole concentration in the device with PMC PSC ( $4.0 \times 10^{16}/\text{cm}^3$ ) is much higher than that of P3HT ( $1.0 \times 10^{16}/\text{cm}^3$ ) and Spiro-OMeTAD PSC ( $1.4 \times 10^{16}/\text{cm}^3$ ). Therefore, the hole density and mobility produce the apparent hole conductivity using  $\sigma = \mu p e$ ,  $8.9 \times 10^{-4}$ ,  $8.1 \times 10^{-4}$  and  $7.5 \times 10^{-3} \text{ S/cm}$  for Spiro, P3HT and PMC PSCs. Thanks to the PMC, the hole conductivity has nearly one order of magnitude larger than traditional molecule HTM and polymer HTM.

Built-in potential can be approximated from the intercept of the linear regime with the x-axis based on the Mott-Schottky plot, which is 0.94 V, 1.04 V and 1.06 V for P3HT, PMC and Spiro-OMeTAD PSC, respectively, well consistent with the value of  $V_{oc}$  in the  $J$ -V curves.

$$C^{-2} = \frac{2(V_{bi} - V)}{A^2 e \epsilon \epsilon_0 N_A} \quad (1)$$

Where  $V_{bi}$  is the built-in potential;  $V$  is the applied bias;  $A$  corresponds to the active area ( $0.1 \text{ cm}^2$ );  $e$  accounts for the elementary charge;  $\epsilon$  is the relative dielectric constant;  $\epsilon_0$  the permittivity of free space, and  $N_A$  is the concentration of carriers.

## CONCLUSION

In summary, we develop a molecule/polymer composite HTM with periodic microstructure through self-assembling. This PMC HTM has dual function in optics and electronics for high performance PSC with ultrathin perovskite layer. First, the PMC in combination with Au electrode affords light cavity for the absorption enhancement and thus thin layer of perovskite can fully extinct the solar spectrum. The light cavity is a coupling of Fabry–Pérot cavity and SPR, amounting to plasmonic cavity to promote the absorption of PSC. Second, the molecule/polymer packing and assembly enhance the hole conductivity through elevation of mobility and carrier concentration, as large as one order of magnitude. Due to high efficient hole extraction and collection, the abnormal hysteresis is reduced compared to standard spiro-OMeTAD. Thanks to the optical and electronic enhancement, the PMC PSC afford high efficiency PSC using ultrathin perovskite layer, delivering a  $V_{oc}$  of 1.05 V,  $J_{sc}$  of 22.9 mA cm<sup>-2</sup>, FF of 0.737, and efficiency amounting to 17.7% PCE, the highest efficiency with as thin as 240 nm perovskite layer.

## MATERIALS AND METHODS

**Perovskite Precursor Synthesis:** CH<sub>3</sub>NH<sub>3</sub>I (MAI) was prepared according to the similar process reported.<sup>10, 45</sup> Briefly, methylamine (CH<sub>3</sub>NH<sub>2</sub>, 33%w/w in ethanol, Sigma-Aldrich) and excess hydroiodic acid (HI, 57%w/w in water, Sigma-Aldrich) were stirred in an ice bath for 2 hrs to get the MAI powders. The powders were recovered by precipitating at 70 °C for 2 hrs. The MAI was dissolved in ethanol and recrystallized with diethyl ether (Sigma-Aldrich) three times before further dried in vacuum at 70 °C overnight.

CH<sub>3</sub>NH<sub>3</sub>PbI<sub>3-x</sub>Cl<sub>x</sub> precursor solution was prepared as 0.83 M lead chloride (99.999%, Sigma-Aldrich) and 2.49 M MAI in anhydrous N, N-Dimethylformamide (DMF, 99.8%, Sigma-Aldrich) and stirred at 60 °C for 4 hrs. Then the precursor was filtered with a PTFE with 0.45 μm pore size. The solution is stored under nitrogen atmosphere at room temperature.

**Solar cells fabrication:** F-doped SnO<sub>2</sub> (FTO) (DHS-FTO22–15N, HeptaChroma) substrates were cleaned in an ultrasonic bath sequentially with acetone, 2-propanol and ethanol for 15 mins, separately. The TiO<sub>2</sub> precursor was prepared by 0.6 mL titanium isopropoxide (Sigma-Aldrich, 99.999%) and 0.15 mL 37%w/w HCl solution dissolved in 15 mL ethanol. The dense TiO<sub>2</sub> film was coated onto FTO substrate by spin-coating of titanium precursor at 5000 rpm for 40 s, followed by annealing in air at 500 °C for 30 minutes.

After the TiO<sub>2</sub> substrates cooled to room temperature, the MAPbI<sub>3-x</sub>Cl<sub>x</sub> precursor was deposited onto TiO<sub>2</sub> substrate by spin-coating at 3500 rpm for 40 s. After drying at room temperature for 10 mins, the films were baked at 100 °C for 1.0 h. The color of the film turned from yellow to black with a mirror-like reflective surface, indicating the formation of MAPbI<sub>3-x</sub>Cl<sub>x</sub>. The spiro-OMeTAD was prepared by dissolving 75 mg spiro-OMeTAD (25 μL lithium-bis(trifluoromethanesulfonyl) imide (Li-TFSI, Sigma-Aldrich,

99.8%) solution (520 mg in 1 mL acetonitrile, Sigma-Aldrich, 99.8%), and 35 μL 4-tert-butylpyridine (Sigma-Aldrich, 96%) in 1ml chlorobenzene. The P3HT (LUM-TEC) was dissolved in 1, 2-chlorobenzene (Sigma-Aldrich, 99.8%) with 15 mg mL<sup>-1</sup>. The binary HTM were prepared by blending the spiro-OMeTAD and P3HT solution with molecule/polymer volume ratios of 1:1, 2:1, 3:1 and 4:1. Hole transport layer was deposited on the annealed perovskite film by spin-coating at 3000 rpm for 40 s. And for the device with spiro-OMeTAD only, the spin coating speed was 5000 rpm for 40 s in order to get the optimized efficiency. The devices were placed in a moisture-controlled cabinet overnight for oxidization of spiro-OMeTAD. Finally, an 80 nm Au layer was deposited by thermal evaporation at a pressure of 3×10<sup>-4</sup> mbar with shadow mask area of 0.1 cm<sup>2</sup>. The perovskite and HTM related steps were carried out in a N<sub>2</sub>-purged glovebox.

**Measurement and Characterization:** The crystalline structure was characterized by XRD (Siemens D5005 with Cu Ka radiation). The general morphologies of the films were characterized by SEM (FEI, Quanta 400). The current density-voltage curves were measured (Keithley Instruments, 2612 Series Source Meter) under simulated AM 1.5 sunlight generated by a 94011A-ES Sol series Solar Simulator. EQE were measured with a Keithley 2400 Source Meter under monochromatic illumination generated by passing the light beam from a 250 W quartz tungsten halogen lamp into a Newport 74215 Oriel Cornerstone 260 1/4 m monochromatic. A calibrated silicon diode with a known spectral response was used as the reference. Absorption and scattering spectra were obtained by UV-vis spectrometer (SHIMADZU UV-3600) equipped with integrating sphere to analyze the optical properties of the HTM. For scattering measurement, the samples were mounted at the backside of the integrating sphere and the reflectance spectra were normalized to the reflection of a white-standard. Atomic force microscope (AFM, Nanoscope IIIa) was operated in tapping mode to acquire the surface morphology of the thin films. The voltage dependent capacitance was measure using a HP 4284.

## Acknowledgements

We thank Prof Shihe Yang in HKUST and Prof Ni Zhao in CUHK for useful discussions. The work is in part supported by Research Grants Council of Hong Kong, particularly, via Grant Nos AoE/P-03/08, N\_CUHK405/12, T23-407/13-N, AoE/P-02/12, CUHK1/CRF/12G, and CUHK Group Research Scheme, as well as Innovation and Technology Commission ITS/096/14. National Science Foundation of China, via Grant No 61229401.

## Notes and references

1. G. Xing, N. Mathews, S. Sun, S. S. Lim, Y. M. Lam, M. Grätzel, S. Mhaisalkar and T. C. Sum, *Science*, 2013, **342**, 344-347.
2. W. Nie, H. Tsai, R. Asadpour, J.-C. Blancon, A. J. Neukirch, G. Gupta, J. J. Crochet, M. Chhowalla, S. Tretiak and M. A. Alam, *Science*, 2015, **347**, 522-525.

3. B. Cai, Y. Xing, Z. Yang, W.-H. Zhang and J. Qiu, *Energy & Environmental Science*, 2013, **6**, 1480-1485.
4. Q. Dong, Y. Fang, Y. Shao, P. Mulligan, J. Qiu, L. Cao and J. Huang, *Science* **2015**, *247*, 967-970.
5. S. D. Stranks, G. E. Eperon, G. Grancini, C. Menelaou, M. J. Alcocer, T. Leijtens, L. M. Herz, A. Petrozza and H. J. Snaith, *Science*, 2013, **342**, 341-344.
6. M. M. Lee, J. Teuscher, T. Miyasaka, T. N. Murakami and H. J. Snaith, *Science*, 2012, **338**, 643-647.
7. N. J. Jeon, J. H. Noh, Y. C. Kim, W. S. Yang, S. Ryu and S. I. Seok, *Nat. mater.* **2014**, *13*, 897-903.
8. H.-S. Kim, C.-R. Lee, J.-H. Im, K.-B. Lee, T. Moehl, A. Marchioro, S.-J. Moon, R. Humphry-Baker, J.-H. Yum and J. E. Moser, *Sci. Rep.* **2012**, *2*, 591.
9. N.-G. Park, *J. Phys. Chem. Lett.* **2013**, *4*, 2423-2429.
10. J. M. Ball, M. M. Lee, A. Hey and H. J. Snaith, *Energy Environ. Sci.* **2013**, *6*, 1739-1743.
11. H. Yu, F. Wang, F. Xie, W. Li, J. Chen and N. Zhao, *Adv. Funct. Mater.* **2014**, *24*, 7102-7108.
12. J. Burschka, N. Pellet, S.-J. Moon, R. Humphry-Baker, P. Gao, M. K. Nazeeruddin and M. Grätzel, *Nature*, 2013, **499**, 316-319.
13. A. Kojima, K. Teshima, Y. Shirai and T. Miyasaka, *J. Am. Chem. Soc.* **2009**, *131*, 6050-6051.
14. N. Pellet, P. Gao, G. Gregori, T. Y. Yang, M. K. Nazeeruddin, J. Maier and M. Grätzel, *Angew. Chem. Int. Ed.* **2014**, *53*, 3151-3157.
15. S. Kazim, M. K. Nazeeruddin, M. Grätzel and S. Ahmad, *Angew. Chem. Inter. Ed.* **2014**, *53*, 2812-2824.
16. Q. Lin, A. Armin, R. C. R. Nagiri, P. L. Burn and P. Meredith, *Nat. Photonics* **2015**, *9* 106-112.
17. J. M. Ball, S. D. Stranks, M. T. Hörantner, S. Hüttner, W. Zhang, E. J. Crossland, I. Ramirez, M. Riede, M. B. Johnston and R. H. Friend, *Energy Environ. Sci.* **2015**, *8*, 602-609.
18. S. N. Habisreutinger, T. Leijtens, G. E. Eperon, S. D. Stranks, R. J. Nicholas and H. J. Snaith, *Nano Lett.* 2014, **14**, 5561-5568.
19. H. J. Snaith, A. Abate, J. M. Ball, G. E. Eperon, T. Leijtens, N. K. Noel, S. D. Stranks, J. T.-W. Wang, K. Wojciechowski and W. Zhang, *J. Phys. Chem. Lett.* **2014**, *5*, 1511-1515.
20. D. Derkacs, S. Lim, P. Matheu, W. Mar and E. Yu, *Appl. Phys. Lett.* **2006**, *89*, 093103.
21. S. Chang, Q. Li, X. Xiao, K. Y. Wong and T. Chen, *Energy Environ. Sci.* **2012**, *5*, 9444-9448.
22. S.-S. Kim, S.-I. Na, J. Jo, D.-Y. Kim and Y.-C. Nah, *Appl. Phys. Lett.* **2008**, *93*, 073307.
23. K. Catchpole and A. Polman, *Opt. Exp.* **2008**, *16*, 21793-21800.
24. W. Zhang, M. Saliba, S. D. Stranks, Y. Sun, X. Shi, U. Wiesner and H. J. Snaith, *Nano Lett.* 2013, **13**, 4505-4510.
25. M. G. Kang, T. Xu, H. J. Park, X. Luo and L. J. Guo, *Adv. Mater.* 2010, **22**, 4378-4383.
26. C. Cocoyer, L. Rocha, L. Sicot, B. Geffroy, R. De Bettignies, C. Sentein, C. Fiorini-Debuisschert and P. Raimond, *Appl. phys. Lett.* 2006, **88**, 133108.
27. R. A. Pala, J. White, E. Barnard, J. Liu and M. L. Brongersma, *Adv. Mater.* 2009, **21**, 3504-3509.
28. C. Battaglia, C.-M. Hsu, K. Söderström, J. Escarre, F.-J. Haug, M. Charrière, M. Boccard, M. Despeisse, D. T. Alexander and M. Cantoni, *ACS nano* 2012, **6**, 2790-2797.
29. I. Ding, J. Zhu, W. Cai, S. J. Moon, N. Cai, P. Wang, S. M. Zakeeruddin, M. Grätzel, M. L. Brongersma and Y. Cui, *Adv. Energy Mater.* 2011, **1**, 52-57.
30. N. J. Jeon, H. G. Lee, Y. C. Kim, J. Seo, J. H. Noh, J. Lee and S. I. Seok, *J. Am. Chem. Soc.* 2014, **136**, 7837-7840.
31. J. H. Heo, S. H. Im, J. H. Noh, T. N. Mandal, C. S. Lim, J. A. Chang, Y. H. Lee, H. J. Kim, A. Sarkar, M. K. Nazeeruddin, M. Grätzel and S. I. Seok, *Nat. Photonics* 2013, **7**, 487-492.
32. R. J. Kline, M. D. McGehee, E. N. Kadnikova, J. S. Liu and J. M. J. Frechet, *Adv. Mater.* 2003, **15**, 1519-1522.
33. J. A. Bartelt, J. D. Douglas, W. R. Mateker, A. El Labban, C. J. Tassone, M. F. Toney, J. M. J. Frechet, P. M. Beaujuge and M. D. McGehee, *Adv. Energy Mater.* **2014**, *4*, 1301733.
34. K. Yan, Z. Wei, J. Li, H. Chen, Y. Yi, X. Zheng, X. Long, Z. Wang, J. Wang, J. Xu and S. Yang, *Small* **2015**, *11*, 2269-2274.
35. K. Yan, M. Long, T. Zhang, Z. Wei, H. Chen, S. Yang and J. Xu, *J. Am. Chem. Soc.* 2015, **137**, 4460-4468.
36. Z. H. Wei, K. Y. Yan, H. N. Chen, Y. Yi, T. Zhang, X. Long, J. K. Li, L. X. Zhang, J. N. Wang and S. H. Yang, *Energy Environ. Sci.* 2014, **7**, 3326-3333.
37. Z. Wei, H. Chen, K. Yan and S. Yang, *Angew. Chem. Int. Ed.* **2014**, *126*, 13455-13459.
38. J.-H. Im, I.-H. Jang, N. Pellet, M. Grätzel and N.-G. Park, *Nat. Nanotechnol.* 2014, **9**, 927-932.
39. K. Yan, L. Zhang, J. Qiu, Y. Qiu, Z. Zhu, J. Wang and S. Yang, *J. Am. Chem. Soc.* **2013**, *135*, 9531-9539.
40. W. Ding, Y. Wang, H. Chen and S. Y. Chou, *Adv. Funct. Mater.* **2014**, *24*, 6329-6339.
41. S.-F. Leung, M. Yu, Q. Lin, K. Kwon, K.-L. Ching, L. Gu, K. Yu and Z. Fan, *Nano Lett.* 2012, **12**, 3682-3689.
42. H. Huang, L. Lu, J. Wang, J. Yang, S.-F. Leung, Y. Wang, D. Chen, X. Chen, G. Shen and D. Li, *Energy Environ. Sci.* **2013**, *6*, 2965-2971.
43. H. Zhou, Y. Zhang, J. Seifert, S. D. Collins, C. Luo, G. C. Bazan, T. Q. Nguyen and A. J. Heeger, *Adv. Mater.* 2013, **25**, 1646-1652.
44. W. A. Laban and L. Etgar, *Energy Environ. Sci.* 2013, **6**, 3249-3253.
45. G. E. Eperon, V. M. Burlakov, P. Docampo, A. Goriely and H. J. Snaith, *Adv. Funct. Mater.* 2014, **24**, 151-157.